First-principles study of crystalline bundles of single-walled boron nanotubes with small diameter

Kah Chun Lau, Roberto Orlando[1] and Ravindra Pandey[2]

Department of Physics, Michigan Technological University, Houghton, MI 49931, USA

E-mail: pandey@mtu.edu

Abstract

First-principles calculations based on density functional theory are performed to study structural and electronic properties of crystalline bundles of $(n, 0)$ zigzag and $(0, n)$ armchair-type single-walled boron nanotubes (SWBNT) with small diameter, about 4–6 Å. The results predict a modification in the properties of SWBNT bundles relative to those of isolated nanotubes with small diameter. The predicted modification can be attributed to a significant interplay between intra- and inter-tubular bonds in determining the stability of bundles of small diameter SWBNT, analogous to the role played by intra- and inter-icosahedral bonds in the boron crystalline solids.

(Some figures in this article are in colour only in the electronic version)

1. Introduction

Elemental boron exhibits rather fascinating chemical versatility which has been well studied in the crystalline solid form, but has scarcely been investigated in nanostructures. First-principles studies have taken the initiative in recent years, reporting some of the energetically competitive configurations of boron sheets and nanotubes [1–3, 5–7]. Among the several possible 2D sheet configurations, ideal and buckled triangular {1212} sheets together with a reconstructed triangular {1221} sheets were found to be energetically favorable for forming a nanotube. Note that the stability of a boron sheet is found to be governed by the competing roles played by the three-center and two-center bonds [1, 3–5, 7], and the instability of a flat triangular sheet is attributed to the presence of partially occupied in-plane antibonding states [4]. The tubular structures generated from the relatively stable sheet configurations were predicted to have novel electronic and mechanical properties [1, 2, 5, 7–10]. For example, ballistic conduction in the single-walled boron nanotubes (SWBNT) was predicted from electron transport calculations [11]. On the other hand, the (n, n) SWBNT were found to be associated with a very low Poisson ratio [1].

Synthesis of SWBNT within the diameter of $\sim$3 nm using Mg-MCM-41 catalyst was recently reported [14]. Since the tubular structures were found to be extremely sensitive to the high energy electron beam, details of their structural morphology are still unknown. The presence of a tubular structure was, however, confirmed by Raman measurements showing the characteristic radial breathing mode at wavenumbers below 500 cm^{-1}.

It is well known that some of the interesting properties of carbon nanotubes (CNT) which can be synthesized as pristine nanotubes appear only in the condensed phase [12, 13] in which they tend to form close-packed bundles [13]. Therefore, it is of great interest to understand how boron nanotubes can be assembled into stable form via inter-tubular interactions in the condensed phase, knowing that the chemical bonding in the boron nanotube is quite different from that in the carbon nanotube [2, 7].

In a recent theoretical study [7], it was suggested that the strain energy and inter-tubular interaction of single-walled boron nanotubes are diameter and chirality dependent, in contrast to the case for carbon nanotubes. Following this suggestion, we have considered a specific case of SWBNT with small diameter to investigate their morphological evolution in the close-packed bundles in the crystalline phase. Specifically, we will study bonding, stability, thermodynamic, and electronic properties of SWBNT bundles using the state-of-the-art density functional theory. The calculated results show that

---

[1] Permanent Address: Dipartimento di Scienze e Tecnologie Avanzate, Università del Piemonte Orientale, Via Bellini 25/G, 15100 Alessandria, Italy.
[2] Author to whom any correspondence should be addressed.

Table 1. Boron sheet configurations: buckled and idealized {1212}, and reconstructed {1221} configurations: binding energy BE (eV/atom) and the bond lengths (R_{B-B}).

Ref.	Model	Idealized {1212} BE	Idealized {1212} R_{B-B} (Å)	Buckled {1212} BE	Buckled {1212} R_{B-B} (Å)	Reconstructed {1221} BE (Å)	Reconstructed {1221} R_{B-B} (Å)
(This work)	GGA	5.37	1.71	5.62	1.62, 1.84	5.48	1.63, 1.69, 2.18
Ref. [3]	LDA	6.36	1.69	6.54	1.60, 1.83	6.33	1.62, 1.64, 1.92
	PAW–LDA	6.39	1.70	6.57	1.60, 1.83	6.37	1.62, 1.65, 1.97
Ref. [3]	GGA	5.48	1.71	5.70	1.61, 1.89	5.57	1.63, 1.66, 2.00
	PAW–GGA	5.69	1.71	5.92	1.61, 1.88	5.78	1.63, 1.66, 2.01
Ref. [1]	LDA	6.53	—	6.79	—	—	—
Ref. [5]	LDA	6.06	1.70	6.27	1.63, 1.81	—	—
Ref. [7]	LDA	6.76	1.69	6.94	1.60, 1.82	—	—
Ref. [5]	GGA	5.49	1.71	5.72	1.64, 1.82	—	—

the subtle interplay between two-centered σ and three-centered π bonds found in the idealized and reconstructed boron sheet configurations yields different morphological features of the corresponding bundles of both zigzag and armchair chiralities, and the presence of a relatively strong inter-tubular interaction modifies stabilities, structural and electronic properties of SWBNT of small diameter in the crystalline bundles.

2. Method

First-principles calculations were performed on the crystalline bundles of SWBNT in the framework of all-electron density functional theory (DFT) with the Perdew–Wang 91 exchange–correlation functional form [15]. The periodic linear combination of atomic orbitals (LCAO) approximation as embedded in the CRYSTAL03 [16] program was employed. A linear combination of Gaussian-type orbitals (GTO) was used to construct a localized atomic basis from which Bloch functions were constructed by a further linear combination with plane-wave phase factors. This LCAO-DFT approach has been successfully applied to a wide variety of materials to study their structural and electronic properties [17].

For our calculations, we begin with a split valence basis set with polarization functions derived from molecular standard 6-31G for boron atoms. The exponents for the most diffuse sp and d shells of this basis set were optimized[3] within

---

[3] The optimized basis set for boron is

6-31G(d, p)
S 6 1.00

$0.206\,888\,2250 \times 10^4$	$0.186\,627\,4590 \times 10^{-2}$
$0.310\,649\,5700 \times 10^3$	$0.142\,514\,8170 \times 10^{-1}$
$0.706\,830\,3300 \times 10^2$	$0.695\,516\,1850 \times 10^{-1}$
$0.198\,610\,8030 \times 10^2$	$0.232\,572\,9330$
$0.629\,930\,4840 \times 10^1$	$0.467\,078\,7120$
$0.212\,702\,6970 \times 10^1$	$0.363\,431\,4400$

SP 3 1.00

$0.472\,797\,1071 \times 10^1$	$-0.130\,393\,7970$	$0.745\,975\,7990 \times 10^{-1}$
$0.119\,033\,7736 \times 10^1$	$-0.130\,788\,9510$	$0.307\,846\,6770$
$0.359\,411\,6829$	$0.113\,094\,4480 \times 10^1$	$0.743\,456\,8340$

SP 1 1.00

$0.160\,000\,0000$	$0.100\,000\,0000 \times 10^1$	$0.100\,000\,0000 \times 10^1$

D 1 1.00

$0.600\,000\,0000$	$0.100\,000\,0000 \times 10^1$

Table 2. α-B_{12} boron: binding energy (BE (eV/atom)) and geometrical parameters. d_{intra} is the intra-icosahedral bond length, d_{inter} is the inter-icosahedral one, and a is the lattice parameter. The unit is Å.

Model		BE	d_{intra}	d_{inter}	a
GGA	(This work)	6.18	1.74, 1.78, 1.80	1.67, 2.01	5.05
	Ref. [3]	6.18	1.74, 1.77, 1.80	1.66, 2.00	5.04
	Ref. [5]	6.22	—	—	—
	Ref. [18]	6.95	—	1.67, 1.99	4.98
	Ref. [19]	—	1.72, 1.76, 1.78	1.65, 1.98	4.98
LDA	(Ref. [7])	7.51	—	—	—
	Experiment [20, 21]	5.81	—	1.71, 2.02	5.06

the convergence of ∼1 mHartree from minimizing the total energy of the {1212} boron sheet which has been previously studied [1–3, 5, 7]. The Brillouin zone was sampled using a $8 \times 8 \times 8$ Monkhorst–Pack grid for the integration in the reciprocal space. The total energy tolerance of 10^{-7} Hartree and eigenvalue tolerance of 10^{-6} Hartree in the iterative solutions of the Kohn–Sham equations were set.

The reliability of the modeling parameters including the optimized basis set was tested considering the competing low-lying configurations of a boron sheet, namely idealized {1212}, buckled {1212} and reconstructed {1221} sheet configurations [1–3, 5, 7]. As shown in table 1, the results of the present study for idealized and buckled {1212} sheet configurations are essentially found to be consistent with the structure models of previous studies [1, 3, 5, 7].

Additionally, the optimized basis set was also tested on the well-studied boron crystalline solid, α-B_{12}. As shown in table 2, the calculated values compare well with the experimental and previously reported values of geometrical parameters of α-B_{12}. For example, the calculated lattice constant of α-B_{12} is 5.05 Å as compared to the experimental value of 5.06 Å [20, 21]. The calculated indirect band gap 1.64 eV agrees well with the previous theoretical [18, 22, 23] (within range of 1.43–1.72 eV) and experimental [24] (∼ 1.9 eV) values.
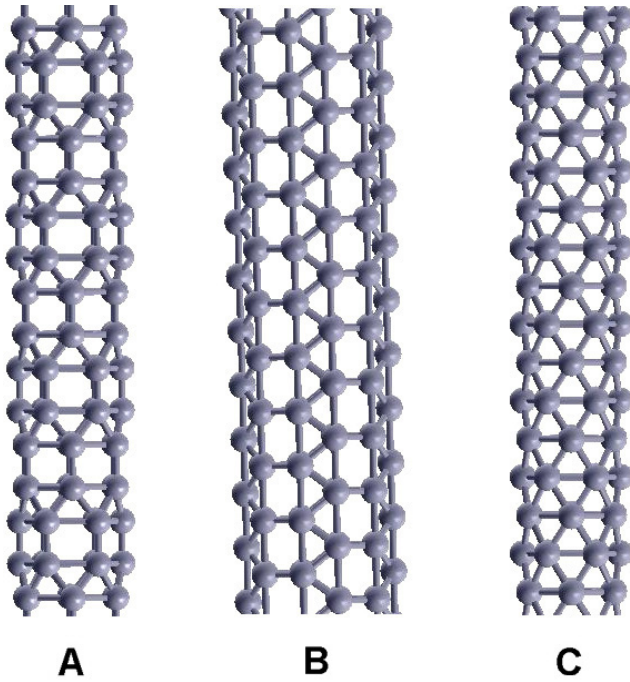
Figure 1. Some of the possible configurations of pristine single-walled boron nanotubes considered for calculations: (A) (6, 0) zigzag type I, (B) (0, 6) armchair type II, (C) (0, 6) armchair type III.

3. Results and discussion

3.1. SWBNT

We have considered several possible configurations, shown in figure 1, of pristine SWBNT [1–3, 5, 7] for electronic structure calculations. Here, we have used the convention established for CNT [25, 26] to describe SWBNT derived from the corresponding 2D sheet configurations.

It must be pointed out that the prototypes of boron sheets proposed in the previous studies [1, 3, 5, 7] have not been observed experimentally. The results of our previous study which performed an extensive search to determine the competing sheet configurations [3] suggest them to be buckled {1212}, idealized {1212} and reconstructed {1221} sheet configurations. Our results on the buckled and idealized {1212} [3] sheet configurations are consistent with the previous studies [1, 2, 5, 7]. Moreover, the reconstructed {1221} boron sheet [2, 3] can be visualized as an assembly of the ground state configuration of the B_6 unit in D_{2h} symmetry. It is stabilized by the presence of the anisotropic bonding with the localized σ bond (i.e. 1.63 Å, table 2) along the armchair direction, and delocalized 3c bonds lying on the zigzag direction within the 'triangular–square–triangular' lattice. Thus the (6, 0) zigzag type I SWBNT (figure 1(A)) can be characterized by a sixfold axis symmetry within the rod group [16] $P6/mmm$. Similarly, the (0, 6) armchair type II SWBNT (figure 1(B)) derived from the reconstructed {1221} boron sheet [3] is associated with the rod group $P\bar{3}1m$ and D_{3d}^1 symmetry.

For the triangular lattice based idealized and buckled {1212} boron sheet derived boron nanotubes, a structure model with well-defined classification schemes has been given

recently [7]. For the highly symmetrical configuration of the idealized {1212} boron sheet in a perfect triangular lattice [1–3, 5, 7], the $(n, 0)$ zigzag and $(0, m)$ armchair type III (figure 1(C)) should be equivalent configurations. However when the puckering is induced to break the symmetry of the idealized {1212} boron sheet [1, 3, 5, 7], a proper classification scheme is needed in the present study.

Instead of triangular [1] and honeycomb derived [5] primitive cells, we therefore adopt the rectangular primitive cell as suggested by Kunstamann *et al* [7] to characterize the SWBNT configurations which derived from buckled {1212} boron sheet. Here, the wrapping vector W^r is defined as [7]

$$W^r = (k, l) = k\mathbf{a}_1^r + l\mathbf{a}_2^r \tag{1}$$

with k, l being integers, and $a_1^r = A(1, 0)$ and $a_2^r = B(0, 1)$ the primitive vectors of the rectangular lattice, where the A and B are the lattice constants. Similar to type I and type II SWBNT, the (0, 6) armchair type III (figure 1(C)) and (0, 6) armchair type IV SWBNT (not shown) in the current study are derived from the idealized and buckled {1212} boron sheet configurations, respectively [1–3, 5, 7]. Both type III and type IV SWBNT belong to the rod group of $P6/mmm$, but are different in terms of the crystallographically non-equivalent B atoms. Note that the diameter of all the tubular configurations considered here is about 4–6 Å. Following the suggestion of Kunstmann *et al*, we do not consider zigzag type IV SWBNT configurations which are less likely to be stable [7].

Electronic structure calculations were performed on the tubular configurations optimizing their lattice parameter as well as the internal coordinates at each fixed value of crystallographic unit-cell volume. The calculated results show that the SWBNT considered are stable, except the (0, 6) armchair type IV SWBNT which makes a transition to a (6, 0) armchair type III SWBNT during the optimization process. This is consistent with the fact that puckering of the boron sheet is not favorable in forming a small diameter armchair SWBNT due to its high curvature strain energy. This result agrees well with the earlier studies [1, 7] in predicting a smooth surface for the armchair SWBNT in the small radii regime. Here within the small radii regime, we found that the type I SWBNT is stable over the type III by nearly 0.42 eV/atom. Knowing the fact that inter-tubular interactions are expected to play an important role in determining the stability of the system [7], we therefore carry on our studies of SWBNT bundles based on these two distinct BNT species.

3.2. Crystalline bundles of SWBNT

Considering the fact that inter-tubular interactions are expected to play an important role in determining the stability of the SWBNT bundles [7], two distinct morphologies of SWBNT bundles consisting of type I (6, 0) zigzag and type III (0, 6) armchair SWBNT with small diameter are considered for electronic structure calculations. The crystalline bundles of SWBNT were represented by arrays of identical nanotubes arranged in a hexagonal lattice. The tubes are of infinite length and not capped. In a hexagonal unit cell, a is defined as the sum of the diameter of the nanotube and its inter-tubular distance, and c represents the periodicity of a SWBNT along its tubular axis.

Table 3. Structural parameters and cohesive energy (E_{coh}) of the SWBNT bundles. R_{B-B}^{inter} and R_{B-B}^{intra} are inter-tubular and intra-tubular distances, and V_0 is the primitive cell volume. $\epsilon^{\alpha-B_{12}}$ is the stability of the system relative to the cohesive energy of α-B_{12} boron solid.

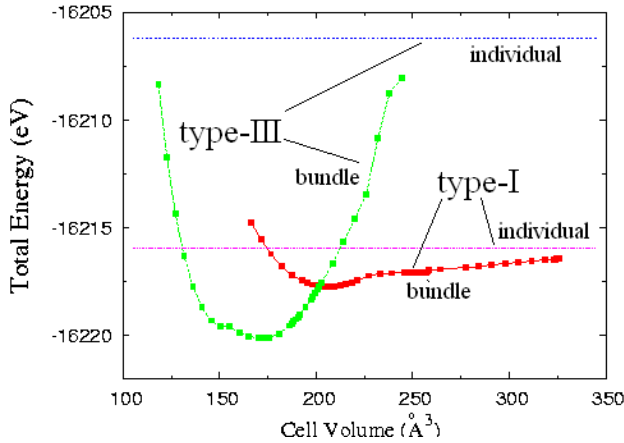| System | | | | Structural parameters | | | Stability | |
(SWBNT bundles)	Configuration	Space group	lattice a, c (Å)	V_0 (Å^3)	R_{B-B}^{inter} (Å)	R_{B-B}^{intra} (Å)	E_{coh} (eV/atom)	$\epsilon^{\alpha-B_{12}}$ (%)
(6, 0) zigzag	Sparse	$P6/mmm$	6.92, 5.93	246	2.96	1.65, 1.98	5.51	89
Type I	Equilibrium	$P6/mmm$	6.21, 5.93	198	1.94	1.63, 1.91	5.58	90
(0, 6) armchair	Sparse	$P6/mmm$	7.19, 5.86	262	3.06	1.75, 1.83	5.09	82
Type III	Equilibrium	$P6/mmm$	5.68, 5.86	163	1.74, 1.98	1.65, 1.79, 1.97	5.68	92

Figure 2. The energy surface represented by total energy versus cell volume in different regimes, namely the sparse and equilibrium configurations of both type I and type III SWBNT bundles. In the sparse region, the cell volume is $\geqslant 240$ Å^3 associated with $R_{B-B}^{inter} \geqslant 3.0$ Å. A straight line represents the total energy of isolated boron nanotubes.

3.2.1. Structural properties. Figure 2 shows the calculated potential energy surface (i.e. total energy versus volume) of the bundles where the lattice parameters as well as the internal coordinates of the tubular configuration were optimized at each value of the unit-cell volume on the energy surface. It was followed by the optimization of the tubular configuration without using any symmetry constraint during the optimization. As shown in figure 2, the sparse configuration on the energy surface is defined as a configuration where a bundle consists of weakly interacting SWBNT with $R_{B-B}^{inter} \geqslant$ 3 Å. On the other hand, the equilibrium configuration is associated with the lowest total energy of a given type of bundles. The calculated equilibrium volume is 200 and 165 Å^3 for type I and type III bundles, with cell density 2.22 and 2.69 g cm^{-3} respectively. Table 3 collects structural and geometrical features of the bundles associated with the sparse and equilibrium configurations on the energy surface shown in figure 2.

There appears to be a crossover of the stability of bundles as the inter-tubular interaction becomes stronger between SWBNT with small diameter. As the overall trend, type I bundles are more stable in the sparse configuration due to their high stability in static energy as pristine nanotubes (section 3.1), whereas type III bundles become more stable

in the equilibrium configuration by settling down in rather compacted, interlinked bundles as shown in figure 3. This fact is reflected in a relatively large change of the cohesive energy of type III bundles ($\sim$0.59 eV/atom) in going from the sparse configuration to the equilibrium configuration (table 3, figure 2), gaining almost 10% of cohesive energy relative to α-B_{12} solid. For the small diameter SWBNT, it is noteworthy that type III SWBNT is not energetically preferable relative to type I SWBNT, though a relatively stronger inter-tubular interaction within the bundles is crucial in stabilizing type III bundles over type I bundles. In fact, our prediction is consistent with the results of a previous study [7] predicting the same order of gain in energy ($\Delta E_{coh} \sim$ 0.30 eV/atom) for a larger diameter (i.e. $\sim$6–12 Å) armchair SWBNT bundles. Such a large gain in cohesive energy clearly points to the fact that inter-tubular interaction in the SWBNT bundles is different from that in the carbon nanotube bundles, which are bonded by weak van der Waals interactions [27].

3.2.2. Bonding. In type I SWBNT, the chemical bonding is dominated by the localized two-centered (2c) σ bonds along the tubular direction, whereas the delocalized three-centered (3c) π bonding features with nearly homogeneous electron distribution describe the bonding in type III SWBNT (figure 4). The 'three-centered' bond (3c) generally involves two electrons in a molecular orbital (MO) formed by three atomic orbitals (AO), which yields triangular face configurations (i.e. a triangular B–B–B unit) [28, 29]. In order to extract this unique feature of bonding in boron nanostructures, we use Mulliken population analysis, together with electronic charge density maps for the SWBNT and crystalline bundles considered.

In the sparse configuration of the crystalline bundles, there is almost no total charge density distribution in the inter-tubular region as shown in figure 5. The total charge density is nearly equivalent to the superposition of charge densities of individual pristine nanotubes. For bundles in the equilibrium configuration, we use the Mulliken population analysis to estimate the strength of the intra-tubular and inter-tubular bonds in terms of the degree of overlap population $b(A^0, B^0)$ in units of e among the nearest neighbors.

Table 4 collects the values of $b(A^0, B^0)$ associated with the atoms in either intra-tubular or inter-tubular bonding regions of the crystalline bundles. In type I bundles, there is a dominance of the σ bonds which interconnect the 'triangle–square–triangle' along the tubular axis over the π bonds
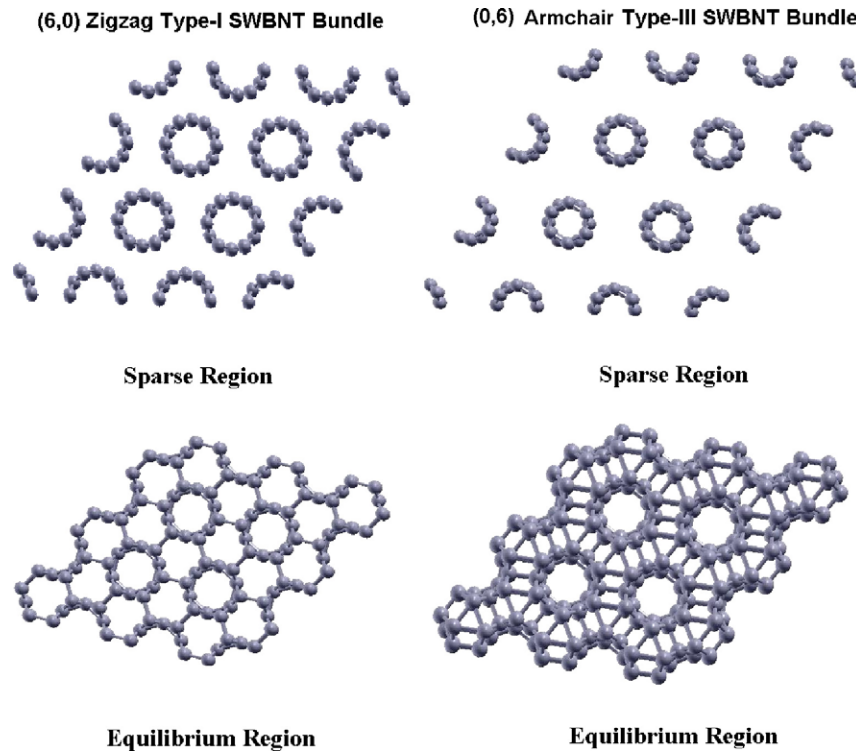
Figure 3. A top view of type I and type III crystalline bundles of SWBNT in the sparse and equilibrium configurations.
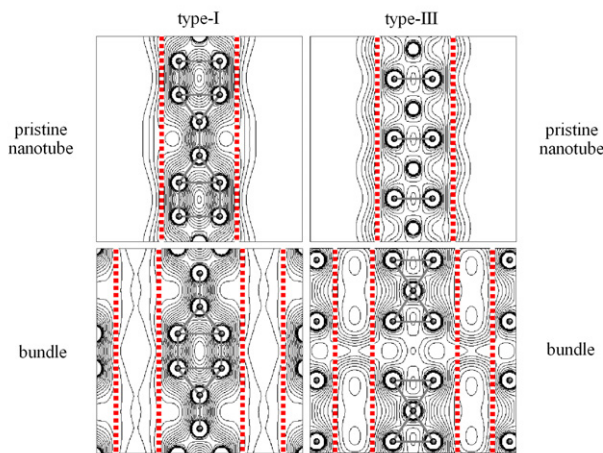

Figure 4. A side view of the electronic charge density maps on the 2D plane along the tubular axis of pristine SWBNT and crystalline bundles at the equilibrium configurations. Top: (left) (6, 0) zigzag type I SWBNT, (right) (0, 6) armchair type III SWBNT. Bottom: (left) (6, 0) zigzag type I and (right) (0, 6) armchair type III SWBNT based crystalline bundles. The red dotted lines represent the outline of the side view of each tubules.

associated with the boron atoms along the triangular network in the intra-tubular region. The 2c bonds in the crystalline bundles, therefore, appear to be as rigid as those in isolated nanotubes.

For type III bundles, the inter-tubular interaction is described by both 2c and 3c bonds, both having significant strength. Interestingly, the strength of 3c bonds is nearly

the same in both inter- and intra-tubular regions (table 4). Furthermore, a presence of 'buckling' induced two-centered σ bonds in the intra-tubular and inter-tubular regions of the bundles is confirmed, though they were not present in the isolated type III SWBNT. This is also reflected in a rather large value of about 0.92 of the degree of polygonization (i.e. $\eta = r_s/r_l$, where r_s and r_l are the short and the long radial dimensions of the nanotube cross section, respectively) of SWBNT in type III bundles[4].

The difference in inter-tube interaction between type I and type III bundles is mainly due to differences in their bonding features in the respective pristine SWBNT. In type I SWBNT, the bonding is dominated by two-centered (2c) σ bonds with $b(A^0, B^0) = 0.66\ e$, whereas the bonding features in type III SWBNT are dominated by three-centered (3c) π bonds with nearly homogeneous electron distribution with $b(A^0, B^0) = 0.41\ e$ (i.e. table 4 and figure 4). When we bring the small diameter SWBNT together to form a bundle, the rigid two-centered σ bonds along tubule axial direction in type I SWBNT cannot easily be deformed, leading to a weaker (i.e. $b(A^0, B^0) = 0.33\ e$ from table 4) inter-tube interactions in type I bundles. On the other hand for type III SWBNT bundles, relatively weak two-centered σ bonds lying along the circumferential direction are found easily distorted to yield stronger inter-tubular 2c and 3c bonds (i.e. $b(A^0, B^0) = 0.52$

[4] Although SWBNT assume a circular cross section in an isolated state, they are not likely to remain in the circular shape in bundles where the inter-tubular interactions are not negligible. Quantitatively, the radial deformation can be expressed in terms of the degree of 'polygonization', $\eta = r_s/r_l$, where r_s and r_l are the short and the long radial dimensions of the nanotube cross section, respectively. When the value of η is 1, a perfect circular cross section of a cylindrical nanotube is expected.

Table 4. $b(A^0, B^0)_{intra}$ and $b(A^0, B^0)_{inter}$ are the overlap populations associated with the intra-tubular and inter-tubular bonds, respectively. 2c and 3c are referred to as 'two-centered' and 'three-centered' bonds, respectively. The overlap population among the nearest neighbors is obtained from the Mulliken charge analysis.

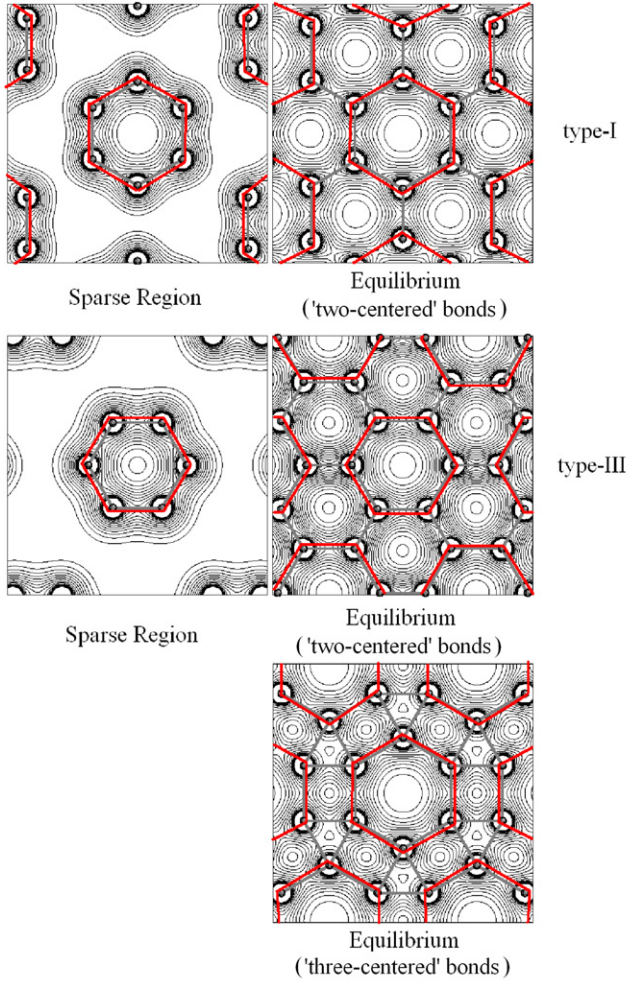| System		Two-centered (2c)		Three-centered (3c)	
(pristine SWBNT/bundle)		$b(A^0, B^0)_{intra}$ (e)	$b(A^0, B^0)_{inter}$ (e)	$b(A^0, B^0)_{intra}$ (e)	$b(A^0, B^0)_{inter}$ (e)
(6, 0) zigzag	Pristine nanotube	0.66	—	0.34	—
Type I	Bundle	0.68	0.33	0.35	—
(0, 6) armchair	Pristine nanotube	—	—	0.41	—
Type III	Bundle	0.32	0.52	0.35	0.36

Figure 5. A top view of the electronic charge density maps on the 2D plane of type I and type III SWBNT crystalline bundles in the sparse and equilibrium configurations. Top: type I bundles. Bottom: type III bundles. The red colored hexagonal box in each figure represents the outline of the top view of SWBNT within the bundle. For type III SWBNT crystalline bundles in the equilibrium configuration, the electronic charge density maps are showing 'two-centered' and 'three-centered' bonds, respectively.

and 0.36 *e*, respectively). This unique bonding character is consistent with the previous study [7] suggesting that distortion of the circumferential σ bonds is expected to enhance the surface chemical reactivity attributed mainly to the unsaturated dangling bonds on the tubular surface for type III SWBNT.

Our results, therefore, suggest that a larger gain in the cohesive energy of type III bundles in going from the sparse to the equilibrium region (figure 2) can be attributed to the presence of a stronger interaction in the inter-tubular region of type III bundles. The buckling of SWBNT in bundles due to the presence of the flexible or 'softer' 3c bonds formed on the tubular surface facilitates the release of the strain of the tubular configurations in bundles. Specifically, the enhanced stability of this system (i.e. $\Delta E_{coh} = 0.59$ eV/atom for small radii SWBNT bundles versus $\Delta E_{coh} \sim 0.30$ eV/atom for large radii SWBNT bundles [7]) via stronger inter-tubular interactions can be attributed to an enhanced reactivity of small diameter armchair type III SWBNT as hypothesized in the recent study [7].

3.2.3. Thermodynamic properties. We use a quasi-harmonic approximation to obtain thermodynamic properties of the SWBNT bundles in which the Debye temperature (Θ_D) is taken to be dependent upon the volume of the crystalline bundles [30]. Accordingly, the calculated potential energy surface (figure 2) is fitted to the well-known Vinet equation of state (EOS) [31] as shown in figure 6. It yields the bulk modulus ($B_0 =$) of 84.9 GPa for type I and 110.5 GPa for type III bundles[5]. The calculated results therefore find the modulus of compressibility for SWBNT crystalline bundles to be significantly higher than that of carbon nanotube based bundles having the bulk modulus of about 42 GPa [37]. In this case, a relatively high modulus of compressibility of SWBNT bundles over SWCNT bundles can be attributed to the dissimilar strength of the inter-tubular interactions in BNT

---

[5] The calculated bulk modulus B_0 for individual SWBNT, using the linear elastic solid model, was found to be in the range of ~100–300 GPa, similar to that for carbon nanotubes (e.g. $B \sim$ 130–260 GPa) [32–35]. Similarly, on the basis of the conventional well-established classical continuum model [12], by assuming extreme disparity between the inter-tube and intra-tube interactions, together with neglecting the coupling between the two interactions in our model initially when inter-tubular separations are large, accordingly we can define B, which is analogous to the deformations in the plane perpendicular to the tubular axis, as [12]

$$B_0 = \frac{(c_{11} + c_{12})}{2} = \frac{A_0^2}{V_0} \frac{\partial^2 E}{\partial A^2}|_{A_0} \qquad (2)$$

where the A_0 and V_0 are the corresponding equilibrium cross section and cell volume of the system. Here the predicted B_0 of type I and type III are 52 and 135 GPa respectively, and match very well with the results that we obtained by fitting to Vinet's equation of state (EOS) [31]. It is important to note that the consistency of these two set values of B_0 for type I and type III SWBNT bundles yielded from these two different models can be compared with B_0 for carbon nanotube bundles on the same footing, since the validity of the model applied to the latter has been well justified [12, 33, 34, 37].
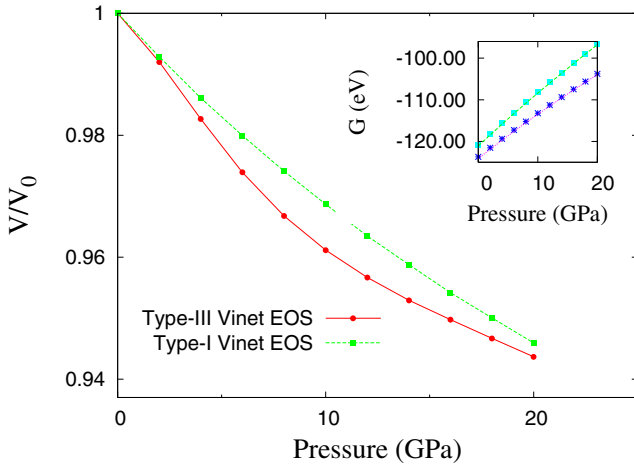
Figure 6. Vinet's equation of states plots for type I and type III bundles. The inset shows the calculated Gibbs energies at 0 and 300 K for both type I and type III bundles.

and CNT. For CNT bundles consisting of SWCNT with radii ~3.8–7.0 Å bundles, the previous studies predict that the pristine CNT interact weakly at separation ~3.1 Å, relative to graphite layers separated at 3.35 Å [34, 37]. On the other hand, the equilibrium configuration of small diameter SWBNT bundles indicates the inter-tube distance, $R_{inter} \sim 1.7$–2.0 Å, and the inter-tube interaction is dominated by relatively strong 2c and 3c bonds as mentioned in the previous section.

The Gibbs function is now minimized with respect to V to obtain the equilibrium volume of the crystalline bundles at constant p and T. As shown in the inset of figure 6, type III bundles become relatively stable with respect to type I bundles as the pressure is increased. The Gibbs free energy difference between type I and type III bundles increases from ~270 to 690 kJ mol^{-1} (i.e. ~2.80–7.15 eV) as we increase the pressure from zero to 20 GPa at 0 K. This trend persists even at 300 K. Overall, a close-packed condensed crystalline phase for the SWBNT bundles is predicted to be thermodynamically stable in the present study.

On the basis of the Debye model [30], the Debye temperature (Θ_D) was calculated using the second derivative of E_{coh}. It is predicted to be 957 and 731 K at zero temperature, and 945 and 704 K at room temperature for type I and type III bundles, respectively. For both crystalline bundles, the calculated Θ_D are found to be less than that of 1219 K for β-boron solid [38], but higher than that of 402 K for graphite [39, 40]. Interestingly, within Debye's model, the temperature dependence of the heat capacity can be well defined by the Debye temperature Θ_D related to the maximum phonon frequency, ν_D in the phonon spectrum. Since the vibrational frequency is always proportional to the square root of the stiffness within the harmonic approximation, Θ_D can be used to characterize the stiffness of a solid, referred to as the 'Debye stiffness' [40]. The Debye stiffness (which is $\propto \Theta_D$) is then related to the hardness (in terms of resistance to plastic deformation) of a material expressed quantitatively in terms of the bulk modulus B_0. Our results for the Debye temperature

Θ_D are consistent with the order of the calculated values for the bulk modulus for both type I and type III BNT bundles ($B_0 = 84.9$ and 110.5 GPa respectively), graphite [34, 40] ($B_0 \sim 28$–39 GPa) and boron solids ($B_0 \sim 185$ and 178–220 GPa for α and β phases, respectively [20, 36]).

3.3. Electronic properties

The crystalline SWBNT bundles show metallic features, similar to the pristine boron nanotubes regardless of composition and chirality. This is in contrast to the case for carbon nanotubes where chirality determines the electronic properties to be metallic or semiconducting. It is to be noted here that the elemental boron nanowires exhibit the semiconducting features [41]. The difference between the electronic properties of bundles and nanowires can be attributed to the distinct local geometric structures of SWBNT as compared to the icosahedral cluster based nanowires [27].

The dispersion of the bands associated with the crystalline bundles in the Brillouin zone responds to the degree of inter-tubular coupling, as expected. It is important to note that the number of available states near Fermi energy can affect the electron transport properties significantly, both in macroscopic and in mesoscopic systems [42]. Accordingly, for the sparse configuration, the band diagram and DOS of the crystalline bundle can be well represented by those for a pristine SWBNT (figure 7). As the inter-tubular interaction becomes dominant, multiple bands associated with intra-tubular and inter-tubular bonds cross at the Fermi level in type I bundles (figure 8).

Considering the ballistic transport [25] consisting of single-electron conduction with no phase and momentum relaxation, the intrinsic quantum conductances of a nanotube can be extracted from its band structure. Therefore, the conductance G is given by the Landauer formula [25]: $G = \frac{2e^2}{h}MT \equiv \frac{2e^2}{h}\sum_{ij}^{M}|t_{ij}|^2$, where T is the transmission probability for a channel, and is given by the sum of transmission probabilities from i th to j th channels, $|t_{ij}|^2$. Assuming that T is constant near the Fermi energy with no electron scattering, the quantized conductance G is proportional to M, which defines the number of channels available for coherent electron propagation in the nanotube.

Accordingly, the ballistic conductance G of each SWBNT considered in the present study can be determined by the number of bands M crossing the Fermi level defined as $G = MG_0$, where $G_0 = \frac{2e^2}{h}$. Thus, in the ballistic limit, the conductance of metallic type I SWBNT [11] is $2G_0$, similar to that associated with the metallic SWCNT. A higher value of the conductance of $5G_0$ associated with type III SWBNT can be attributed to the valence electrons of boron which are shared uniformly forming delocalized 3c bonds, thereby enhancing the probability of electron conduction in the axial direction.

On taking into account of the presence of neighboring nanotubes in a SWBNT bundle, the intrinsic conductance in the 'bulk-like' crystalline bundles is expected to occur along the tubule axial direction (i.e. along Γ–A in figure 8), similarly to that in the corresponding pristine nanotube (figure 7). Here, the conductances of type I and type III bundles are found to be $4G_0$ and $3G_0$, respectively. In type I bundles, the enhanced
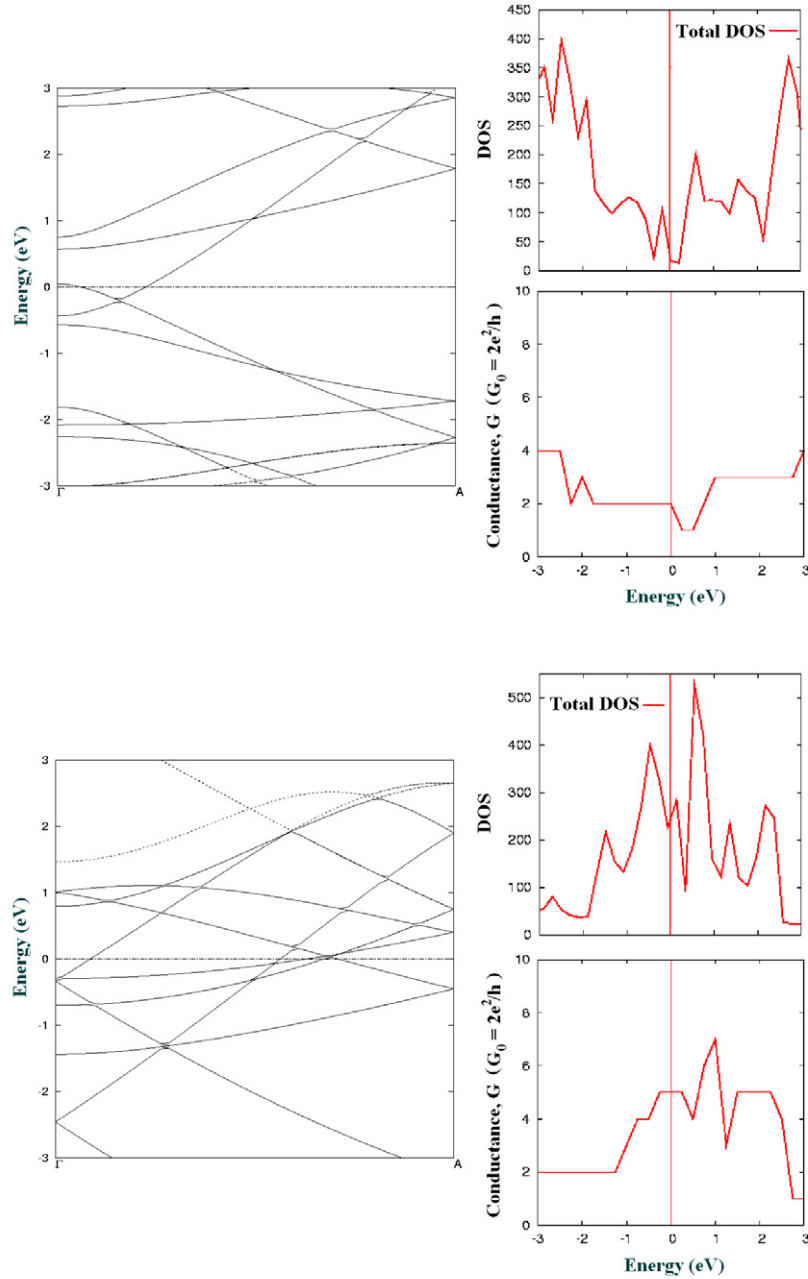
Figure 7. The band structure along tubular axis associated with the Γ-A symmetry line, together with the total density of states (DOS) and intrinsic quantum conductance plot for both type I SWBNT (top) and type III SWBNT (bottom). All plots are plotted within the range of ± 3 eV around the Fermi level E_f, with E_f aligned at zero.

conductances with four conducting channels $\sim 4G_0$ along the tubular direction are attributed to two partially occupied degenerate inter-tubular σ-like and π-like conduction bands, while the three conducting channels of type III correspond to partially occupied p-type non-bonded orbitals crossing the Fermi level. It is also important to note that the intrinsic conductance of a system is purely based on the number of the available states crossing the Fermi level [42], and not necessarily proportional to the strength of interaction. In contrast to the type I bundle case, the strong inter-tubular 2c and 3c bonds found in type III bundles are mostly located in

the occupied valence bands below the Fermi level making no contribution to the intrinsic conductance.

4. Summary

The metallic crystalline bundles of small diameter single-walled boron nanotubes are predicted to be thermodynamically stable with novel properties. The dominance of inter-tubular interactions involving two-centered and three-centered bonding features in SWBNT bundles relative to the Van der Waals interactions yield different structural, mechanical, and
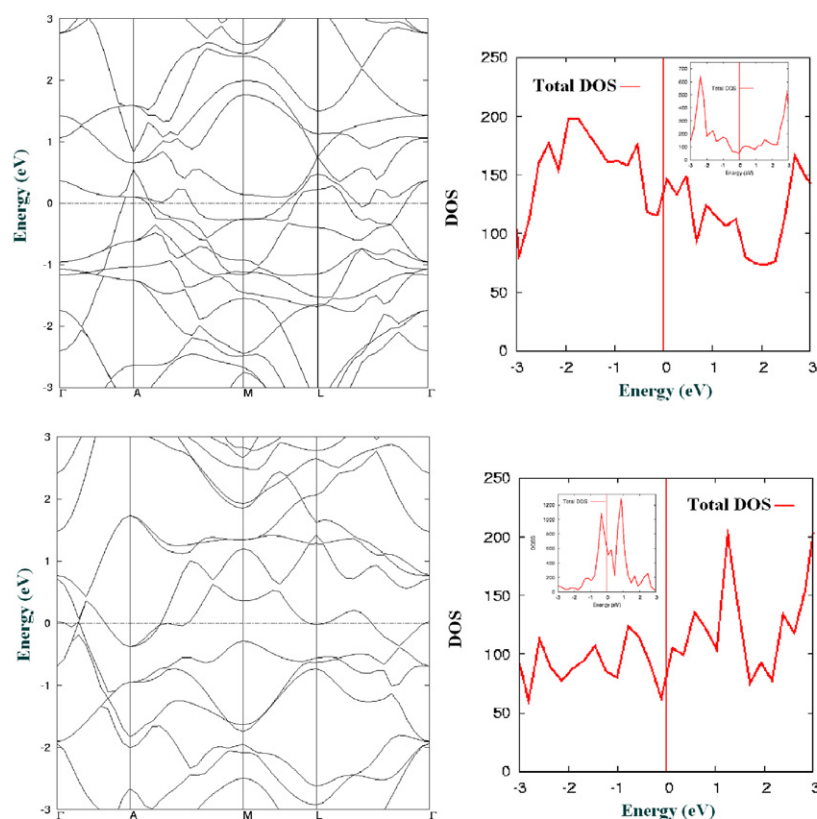
Figure 8. The band structure along the Γ–A–M–L–Γ symmetry line, together with total density of states (DOS) plot for both type I SWBNT (top) and type III SWBNT bundles (bottom). All plots are plotted within the range of ± 3 eV around the Fermi level E_f, with E_f aligned at zero. The insets in the DOS figures shown are the DOS of sparse crystalline bundles for both configurations, which mimic the DOS of pristine SWBNT in both cases.

electronic properties as compared to those associated with isolated SWCNT. Within the small radii regime, it is predicted that if isolated or sparse bundles of small diameter SWBNT are grown, type I bundles based on the reconstructed {1221} boron sheet configuration will be energetically preferred. On the other hand, the close-packed-type III bundles based on the idealized {1212} boron sheet configuration are preferred in the equilibrium configuration. On the basis of the current study on small diameter SWBNT bundles, together with the previous findings from Kunstmann *et al*, scenarios of chiralities and diameters dependent on BNT growth are found to be rather unique among nanotubular systems. Finally, a subtle competition among the intra- and inter-tubular bonds (i.e. among type I and type III SWBNT) appears to lead to polymorphism associated with the boron nanotubes, suggesting that it may be one of the causes of the difficulty in synthesizing SWBNT.

Acknowledgments

References

[1] Evans M H, Joannopoulos J D and Pantelides S T 2005 *Phys. Rev.* B **72** 045434
[2] Lau K C, Pati R, Pandey R and Pineda A C 2006 *Chem. Phys. Lett.* **418** 549
[3] Lau K C and Pandey R 2007 *J. Phys. Chem.* C **111** 2906
[4] Tang H and Ismail-Beigi S 2007 *Phys. Rev. Lett.* **99** 115501
[5] Cabria I, López M J and Alonso J A 2006 *Nanotechnology* **17** 778
[6] Kunstmann J and Quandt A 2005 *Chem. Phys. Lett.* **402** 21
[7] Kunstmann J and Quandt A 2006 *Phys. Rev.* B **74** 035413
[8] Boustani I and Quandt A 1997 *Europhys. Lett.* **39** 527
[9] Gindulytu A, Lipscomb W N and Massa L 1998 *Inorg. Chem.* **37** 6544
[10] Boustani I, Quandt A, Hernández E and Rubio A 1999 *J. Chem. Phys.* **110** 3176
[11] Lau K C, Pandey R, Pati R and Karna S P 2006 *Appl. Phys. Lett.* **88** 212111
[12] Tersoff J and Ruoff R S 1994 *Phys. Rev. Lett.* **73** 676
[13] Salvetat J P, Briggs G A D, Bonard J M, Bacsa R R, Kulik A J, Stöckli T, Burnham N A and Forró L 1999 *Phys. Rev. Lett.* **82** 944
[14] Ciuparu D, Klie R F, Zhu Y and Pfefferle L 2004 *J. Phys. Chem.* B **108** 3967
[15] Perdew J P and Wang Y 1992 *Phys. Rev.* B **45** 13244
[16] Saunders V R, Dovesi R, Roetti C, Orlando R, Zicovich-Wilson C M, Harrison N M, Doll K, Civalleri B, Bush I J, D'Arco P and Llunell M 2003 *CRYSTAL03 User's Manual* Università di Torino, Torino

[17] http://www.crystal.unito.it/
[18] Zhao J and Lu J P 2002 *Phys. Rev.* B **66** 092101
[19] Vast N, Baroni S, Zerah G, Besson J M, Polian A,
     Grimsditch M and Chervin J C 1997 *Phys. Rev. Lett.* **78** 693
[20] Kittel C 1996 *Introduction to Solid State Physics* 7th edn
     (New York: Wiley)
[21] Donohue J 1974 *The Structure of the Elements*
     (New York: Wiley)
[22] Li D, Xu Y and Ching W Y 1992 *Phys. Rev.* B **45** 5895
[23] Lee S, Bylander D M and Kleinman L 1990 *Phys. Rev.* B
     42 1316
[24] Horn F H 1959 *J. Appl. Phys.* **30** 1611
[25] Saito R, Dresselhaus G and Dresselhaus M S 2003 *Physical
     Properties of Carbon Nanotubes* (London: Imperial College
     Press)
[26] Dresselhaus M S, Dresselhaus G and Avouris P (ed) 2001
     *Carbon Nanotubes: Synthesis, Structure, Properties, and
     Applications* (Berlin: Springer)
[27] Quandt A and Boustani I 2005 *Chem. Phys. Chem.* **6** 2001
[28] Muetterties E L (ed) 1967 *The Chemistry of Boron and its
     Compounds* (New York: Wiley)
[29] Muetterties E L (ed) 1975 *Boron Hydride Chemistry*
     (New York: Academic)
[30] Blanco M A, Francisco E and Luaña V 2004 *Comput. Phys.
     Commun.* **158** 57
[31] Vinet P, Rose J H, Ferrante J and Smith J R 1989 *J. Phys.:
     Condens. Matter* **1** 1941
[32] Venkateswaran U D, Rao A M, Richter E, Menon M, Rinzler A,
     Smalley R E and Eklund P C 1999 *Phys. Rev.* B **59** 10928
[33] Lu J P 1997 *Phys. Rev. Lett.* **79** 1297
[34] Reich S, Thomsen C and Ordejòn P 2002 *Phys. Rev.* B
     65 153407
[35] Lu J P 1997 *J. Phys. Chem. Solids* **58** 1649
[36] Nelmes R J, Loveday J S, Allan D R, Besson J M, Hamel G,
     Grima G and Hull S 1993 *Phys. Rev.* B **47** 7668
[37] Tang J, Qin L, Sasaki T, Yudasaka M, Matsushita A and
     Iijima S 2000 *Phys. Rev. Lett.* **85** 1887
[38] Thompson J C and McDonald W J 1963 *Phys. Rev.* **132** 82
[39] Seitz F and Turnbull D (ed) 1964 *Solid State Physics* vol 16
     (New York: Academic)
[40] Tohei T, Kuwabara A, Oba F and Tanaka I 2006 *Phys. Rev.* B
     73 064304
[41] Otten C J, Lourie O R, Yu M, Cowley J M, Dyer M J,
     Ruoff R S and Buhro W E 2002 *J. Am. Chem. Soc.* **124** 4564
[42] Datta S 2003 *Electronic Transport in Mesoscopic Systems*
     (Cambridge: Cambridge University Press)